Eidgenössische Technische Hochschule Zürich
Swiss Federal Institute of Technology Zurich

SED
Schweizerischer Erdbebendienst
Swiss Seismological Service

Report on site characterization

Dagmarselle, Switzerland (DAGMA)

Poggi Valerio, Jan Burjanek, Donat Fäh

Last modified - 24 / 12 / 2014

1. Introduction

In the framework of the NAGRA seismic network project, an array measurement of the ambient vibration wave-field was performed at the location of the SED station DAGMA (Dagmarsellen, Switzerland). The scope of the survey is the seismic characterization of the area surrounding the installation (**Figure 1**), which consists in a broadband seismometer (Trillium Compact) with a high-resolution digitizer (Taurus 24Bit @200sps). Ambient vibration analysis has been used to infer the characteristics of the underground structure of the site, with special regard to the one-dimensional shear-wave velocity. Such profile was later used to assess the local seismic response of the station.

For the analysis, different spectral analysis techniques were implemented, consisting in both single and array methods, which are listed below:

- Time-frequency wavelet analysis
- Power-spectral density estimation
- Conventional horizontal to vertical spectral ratios
- Directional horizontal to vertical spectral ratios
- Wavelet polarization analysis
- Three-component high-resolution f-k analysis.

The results of all these analyses conformed to the definition of the final velocity model. In the following, the main results of these investigations are summarized and a final interpretation of the velocity profile is given. From this interpretation, engineering parameters are finally derived, e.g. the Qwl-Vs average velocity, VsZ (including Vs30) and the seismic amplification from the analytical SH-transfer function of the one-dimensional soil column.

2. Survey description

To characterize the seismic response of the site, an array measurement of ambient vibration was performed on 15/08/2013 (**Figure 1**). The array consists of a single measuring configuration of 14 sensors and about 160m in size. The decision of using a single geometry was taken on the base of the site accessibility. Deploying also a small array close to the SED seismic station was not practically possible, due to the presence of topographic obstacles (a steep slope and the nearby forest, **Figure 2**). A possibility could have been to move such configuration closer to the valley axes, where a flatter area is available, but in this case the result would not have been relevant for the characterization of the seismic station. High velocities were nevertheless expected for the underlying bedrock (Molasse), which is here shallow and in few cases outcropping. This justifies the use of a large geometry for the array to be successful. The maximum aperture of the array was again controlled by the available space in the valley (Lutertal), which was strongly limited toward North and South from dipping slopes. A precise prior estimation of the possible maximum penetration depth was not possible, due to the

large uncertainty of the bedrock velocity, but resolution down to about 100m depth was expected.

During the survey, a total of about two hours of recordings has been acquired. However, not all the stations recorded properly (**Figure 3**). One station (5) did not record at all, probably due to GPS synchronization problems; the sensor of a second station (13) was accidentally badly coupled to the ground, providing too distorted recordings to be subsequently used. The quality of the remaining twelve stations was nevertheless satisfactory, in terms of signal and azimuthal coverage. As it will be better explained later, the sensors have been grouped in two concentric sub-configurations (**Figure 3**). The first configuration includes the most external stations, which are mostly located on rock, while the second (inner selection) samples only the shallow quaternary infill of the central part of the valley.

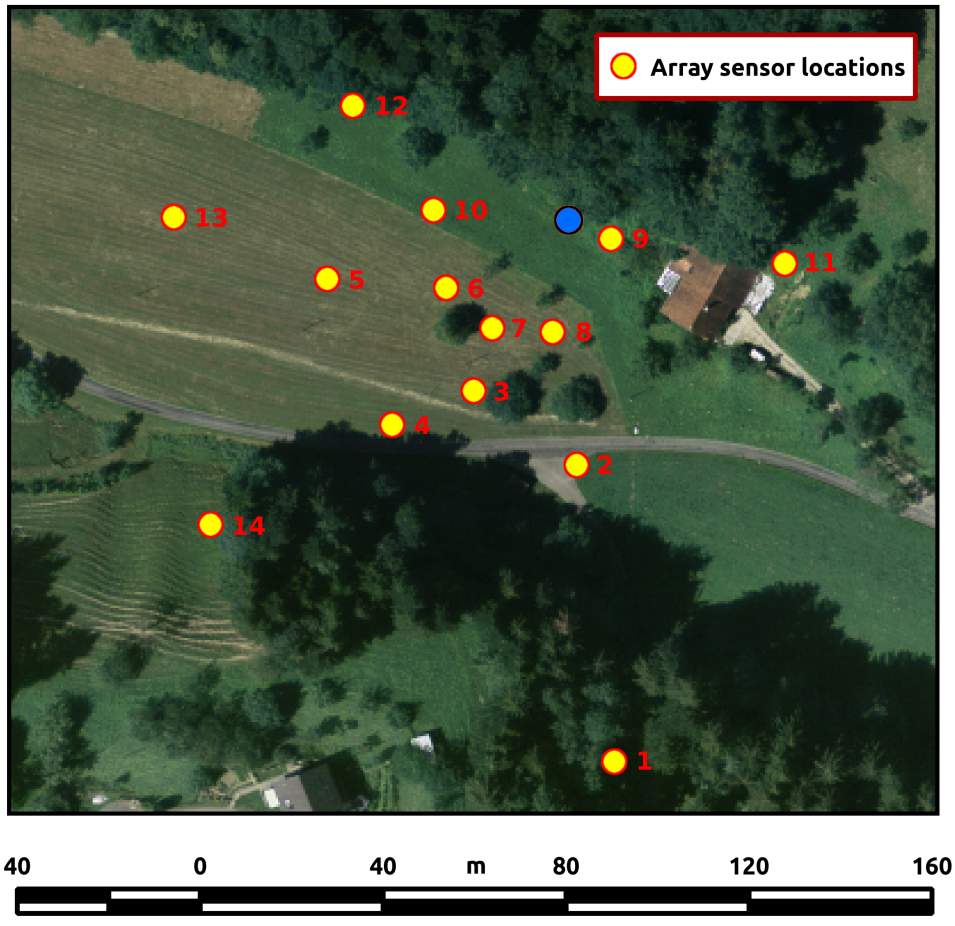

Figure 1 - *Location of the ambient vibration array survey performed in Dagmarsellen (SED station DAGMA) on 15/08/2013. Given the site characteristics, only one array configuration was performed, whose maximum diameter was limited by the available space. The approximate location of the seismic station is shown in blue.*

Figure 2 - *Overview of the measurement area. The array center is roughly located at the center of the picture, while the seismic station DAGMA is on the extreme right, positioned at the edge of the grass field, on a small terrace close to the forest border.*

3. Soil type, topography and geology

The array has been set in open field conditions, in a rural area (**Figure 1**, **Figure 2**). The influence of buildings and anthropogenic disturbances is virtually negligible. Array sensors have been deployed on free soil conditions. Good coupling with the ground was assured by means of digging small holes at the sensor's places, and by using a special support (*Trihedron*®) that facilitates the leveling of the device even for difficult soil conditions. The measurement area is located on a moderate slope dipping toward SSW. However, no topographic correction has been taken into account before processing.

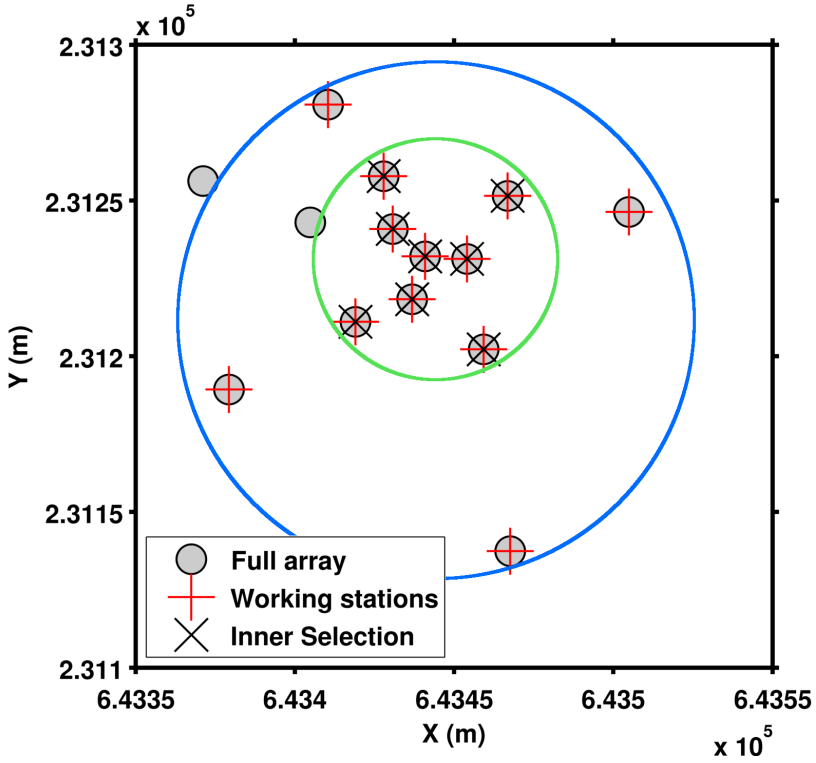

Figure 3 - *Geometry of the ambient vibration array deployed at the station DAGMA. With different symbols are indicated array stations actually used for the processing. The "inner selection" of 8 sensors on the quaternary sediment fill of the valley is also shown.*

From the geological points of view (**Figure 4**), the target area is a small lateral valley incised within the Molasse basin, surrounded by few moranic deposits, clearly identifiable from the surface topography and from the geological map of the area. The central part of such valley is filled by unconsolidated quaternary sediments. The bedrock is very shallow at the measuring location, but rarely exposed across the area (a thin cover of quaternary material is mostly present). The bedrock probably consists of consolidated sandstone with layers of different texture and granulometry, from marl and silt to conglomerate. The surface morphology is considerably smooth and modeled by the action of glaciers during the Pleistocene. Such site can be classified as of rock ground-type A.

4. Acquisition equipment

Each acquisition point within the array consisted of a three components seismometer (Lennartz 3C with 5s eigenperiod) and a 24 bit data logger (Quanterra Q330). Synchronization between stations was assured by standard GPS, while a more accurate differential GPS (Leica Viva system) was used to precisely locate the sensor's coordinates with a tolerance of less than 5cm.

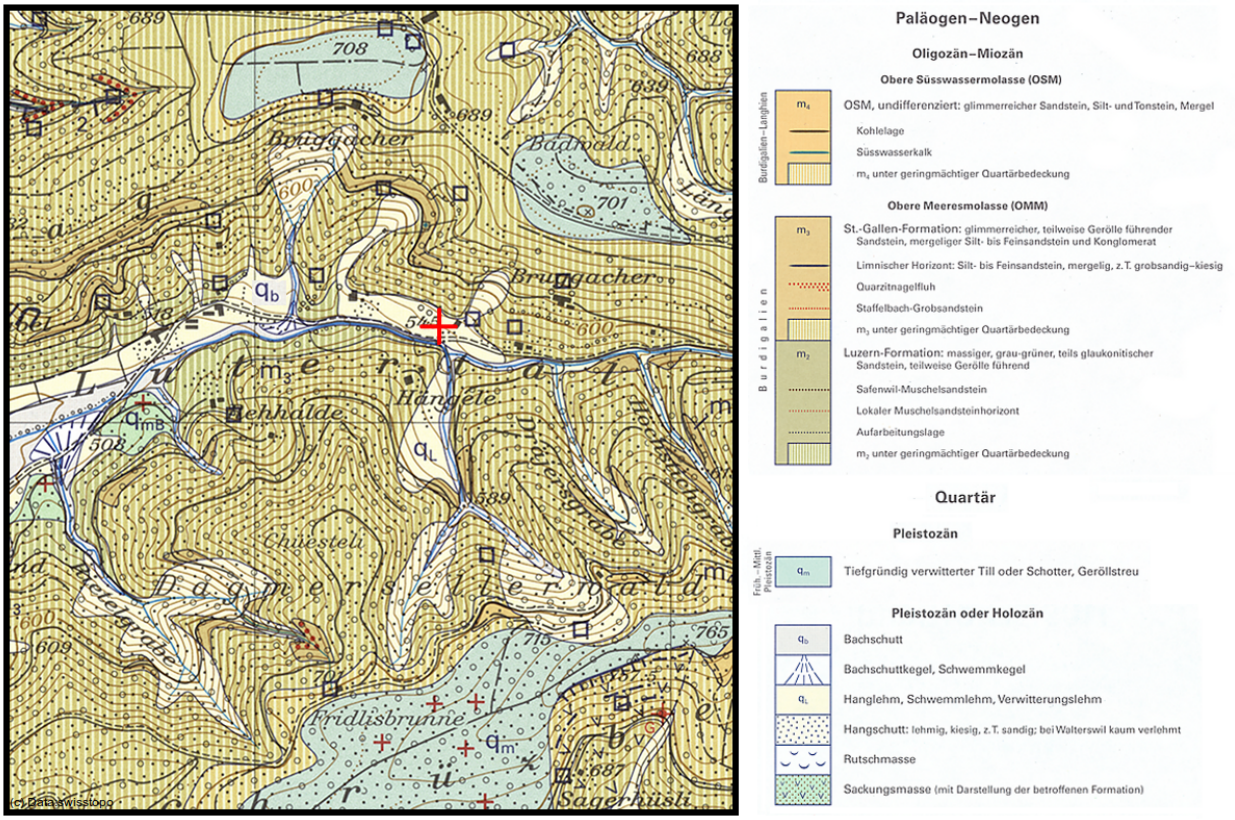

Figure 4 - *Geological map of the Lutertal, in the Dagmarsellen region (reproduced from Swisstopo, modified). In red the approximate location of the permanent station DAGMA.*

5. Weather conditions

The weather conditions were optimal and stable during the whole measurement, with no precipitations, no wind and an average (over the whole day) temperature of 18 degrees.

6. Pre-processing and preliminary data-quality control

The three-component recording has been filtered prior to analysis using a high-pass 6th order causal Butterworth filter with corner at 0.2Hz. Although it is not a strict requirement for spectral analysis techniques, such filtering was applied in order to facilitate the preliminary visual inspection of the noise traces and to evaluate the coherency of the wave-field (**Figure 5**). Such procedure gives essential information for the subsequent interpretation of the f-k analysis results.

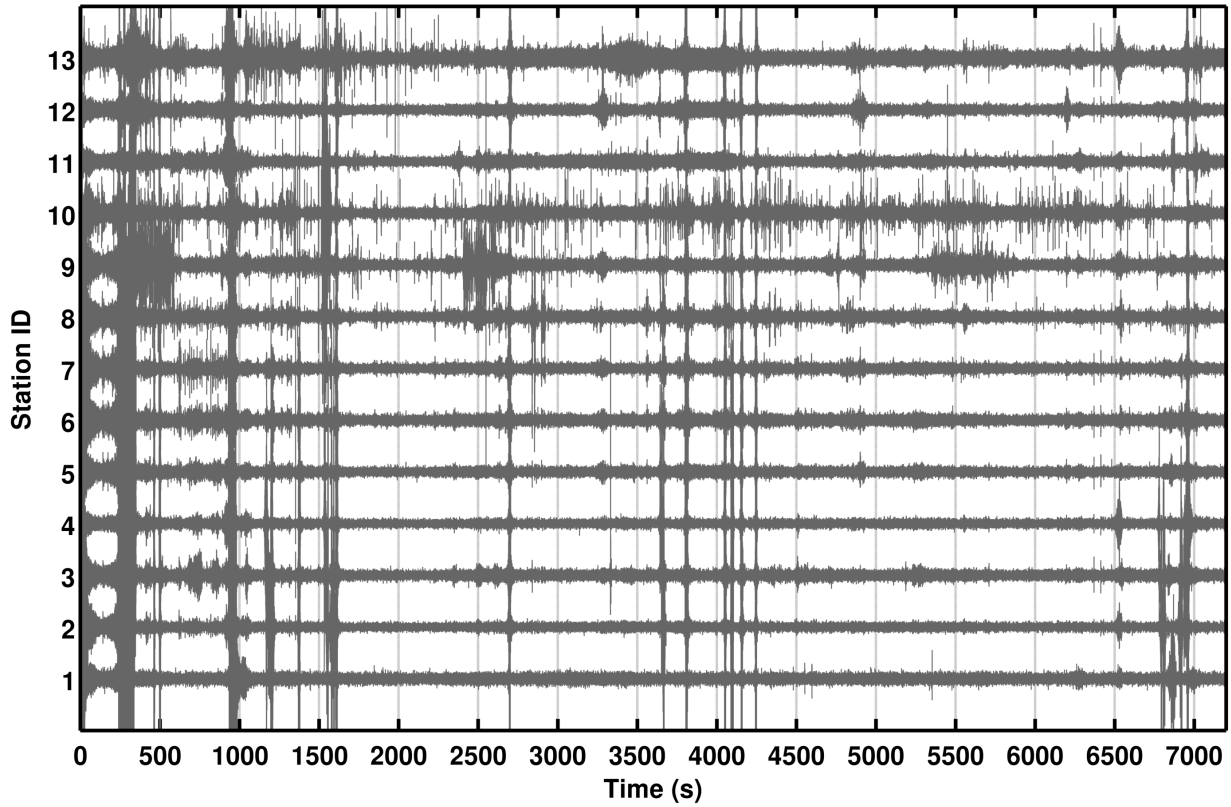

Figure 5 - *Inspection of the useful part of the ambient vibration recording of the array DAGMA. Several impulsive high-frequency transients of anthropogenic origin are visible. Excluding the first 500s of recordings the overall quality of the recording is good.*

To assess the quality of the ambient vibration recordings, spectral analysis was subsequently performed. Because of the stochastic nature of the ambient vibration wave-field, a statistical approach has to be used, such as the estimation of the power spectral density (*PSD*). This approach is useful to evaluate the average energy level of the recordings in the analyzed frequency range, and to access the presence of spurious spectral peaks, which might be related to human activity (machinery, pumps). By inspecting the PSD of the three-component recordings from the whole array in the range between 0.5 and 40Hz, a minor spurious peak is visible at about 14Hz. The peak is more pronounced at the center of the array (**Figure 6** bottom, station 7 - on the sedimentary part) than at the edges (**Figure 6** top, station 1 - on rock) probably because of a resonance. The peak - very narrow - is most likely of anthropogenic origin (from the nearby farm) and should be rejected from interpretation. The average energy level is nevertheless very low, within the minimum and maximum bounds of the USGS noise model.

A) Array Station 1 (on rock)

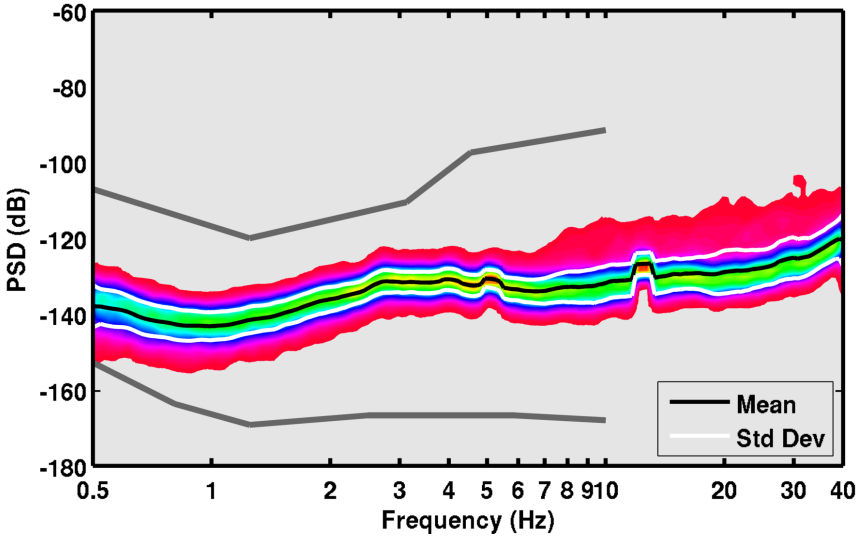

B) Array Station 7 (on sediments)

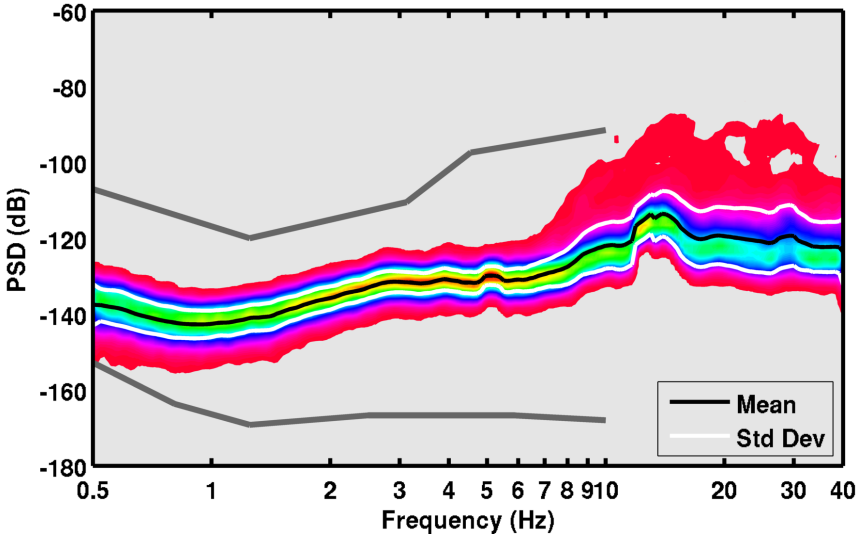

Figure 6 - *Power spectral density (PSD) computed for 2h recording at the central station of the array (station 7) and at the edge of the measuring area (station 1). Similar results were obtained from the other stations of the array. In gray lines are the minimum and the maximum bounds of the USGS noise model, for comparison.*

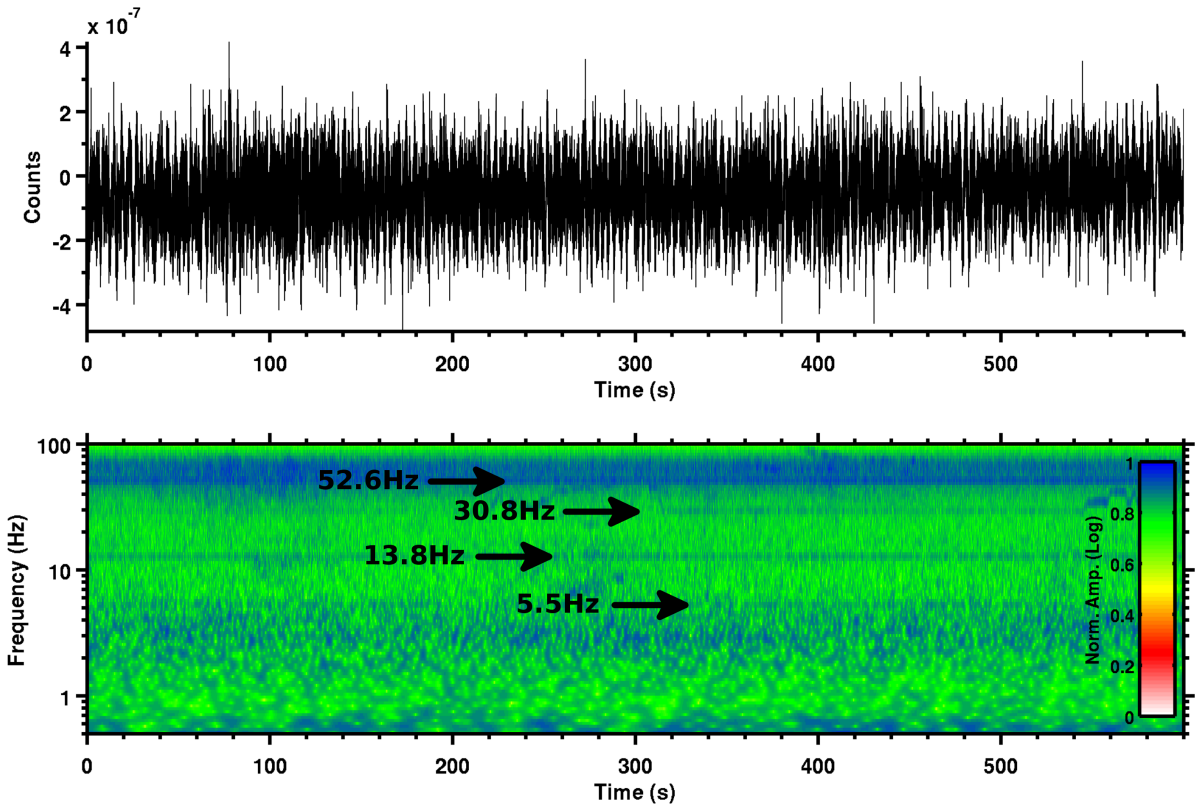

Figure 7 - *Example of spectrogram from 600s of recording of the station number 1 of the array (on rock, vertical component). For the analysis, the cosine wavelet is used (wavelet parameter = 12). Harmonic disturbances are visible on the whole spectrogram, but nevertheless not particularly energetic.*

Complementary to the aforementioned statistical methods, a spectral decomposition approach is more suitable to assess the stationarity of the ambient vibration wave-field over time. The wavelet time-frequency analysis was then performed over the whole recording time. From such analysis (**Figure 7**) an overall stability of the ambient-vibration wave-field over time is evident. The disturbance at about 14Hz is confirmed to be a nearly harmonic contribution, steady over the whole recording window. This provides a further confirmation of its possible anthropogenic origin. Additional harmonic contributions are evident, at 5.5Hz, 30.8Hz and 52.6Hz. These disturbances are nevertheless very weak and well localized in frequency; therefore they won't affect the following processing steps.

7. Conventional H/V spectral ratios

The horizontal-to-vertical (H/V) Fourier spectral ratio is a technique widely used in seismic site characterization because of its ability to provide an estimate of the SH wave fundamental frequency of resonance (f_0) of the site. Other than that, H/V ratios are useful to provide information on the Rayleigh wave ellipticity function, which can be used in the inversion procedure to constrain large velocity contrasts at depth. In this study, we use the H/V technique also to map the variability of the subsoil structure along the investigated area; this is necessary to verify the fulfillment of the 1D structure assumption, which is necessary for the f-k method applied later.

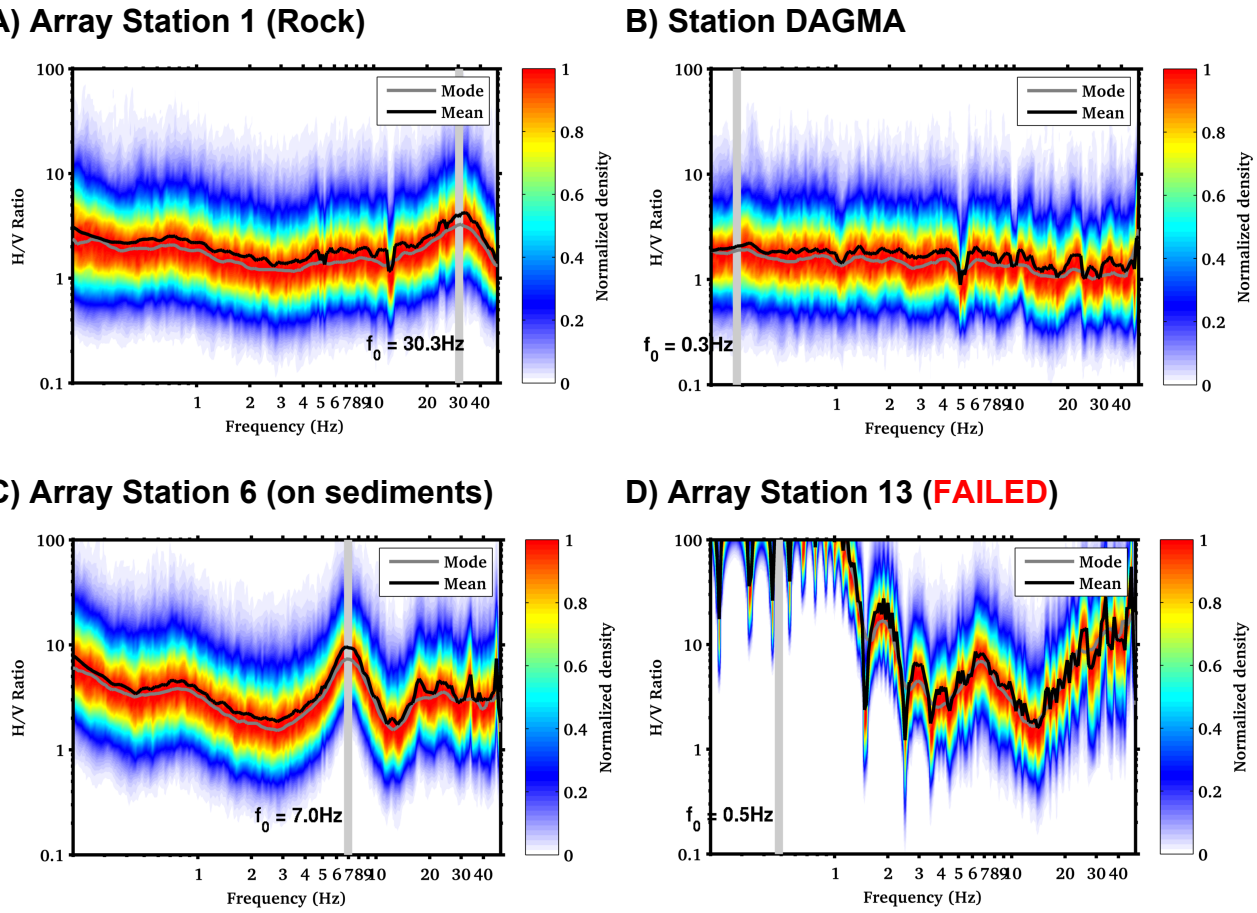

Figure 8 - *Example of H/V spectral ratios at three stations of the array and at the permanent station DAGMA. The bad coupling of the station 13 was evident by inspection of the H/V spectral ratios; this station has not been used for subsequent processing. The resonance frequency of the soil cover is indicated with a light gray line.*

H/V spectral ratios have been computed for the recordings at each station of the array and at the SED permanent station (e.g. **Figure 8**). The behavior of the noise wave-field at the different stations location reflects the characteristic of the valley morphology (**Figure 9**). A high frequency peak is evident over the whole array, however its frequency and amplitude increases moving accordingly from the valley axes, where the thickness of the quaternary deposits is larger, to the edges of the array, where the bedrock is shallower (**Figure 10**). This peak can definitely be used to map the variability of the quaternary fill over the measuring area (e.g. **Figure 11**). Therefore, a simple one-dimensional approximation is not sufficient to explain the high-frequency part of the wave-field (> 7Hz). Conversely, below 7Hz the wave-field is more stable, confirming the homogeneity of the underlying rock. A weak peak is also present at low frequency (< 1Hz), but the interpretation is of more difficult. Such maximum might be induced by a change in lithology within the profile at depth, which causes a modest contrast of seismic impedance. It is also interesting to compare the results of H/V analysis between a typical array station on rock (e.g. **Figure 8**,A) and the permanent station (**Figure 8**, B); the DAGMA station does not show evidence of any high frequency peak, as the sensor has been properly deployed removing the topmost part of the soil cover, which is however resonating in the array recordings.

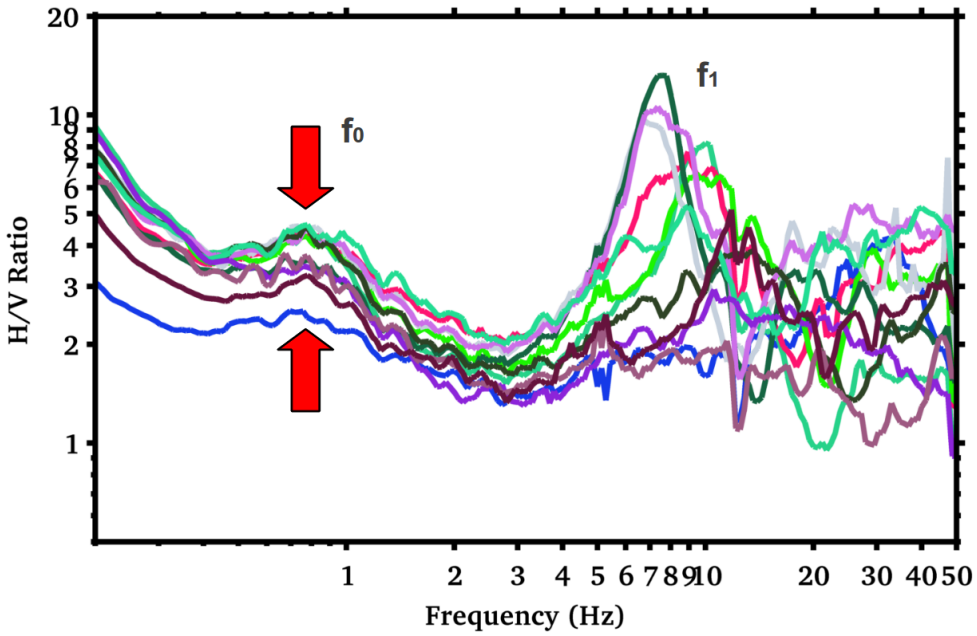

Figure 9 - *Comparison of the H/V spectral ratio curves of all the stations of the array. The curves are stable up to at least 7Hz, confirming the lateral homogeneity of the underlying bedrock velocity structure of the site. A low frequency peak is visible at about 0.8Hz. At high frequencies the spectral ratios are very variable across the array. This reflects the complex geometry of the quaternary sediments cover.*

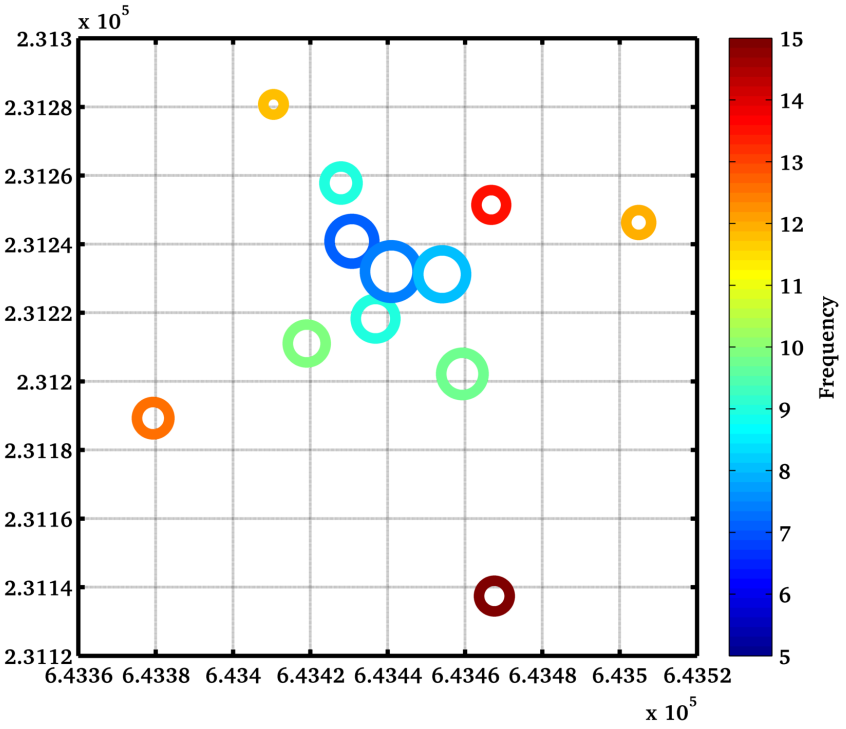

Figure 10 - *Mapping the variation in frequency (with different color) and amplitude (with circles of increasing size) of the high frequency peak (f_1) across the array. It is evident a clear trend from the center of the array to the edges, which reflects the complexity of the quaternary soil cover geometry.*

8. Directional H/V spectral ratios

The computation of directional H/V spectral ratio or polarization analysis is useful to reveal asymmetries in the ambient vibration wave-field. Different effects can induce such a behavior: 2D/3D structure, topographic effects or a non-homogeneous distribution of the noise sources. If a strong directionality is found by the analysis, it is generally recommended to carry out further investigations to properly address the origin of polarization.

By processing the directional H/Vs at all the recording stations of the array (e.g. **Figure 12**) it is possible to observe an isotropy of the wave-field in the low frequency range, roughly below 7Hz. At high frequencies, however, the variability of the H/V peak observed in **Figure 9** is noticeable also in their directionality. As already introduced, this can be explained by the variability of the uppermost soil cover layer over the study area, and should not be interpreted as an effect of non-homogenous distribution of the noise sources. This issue is later investigated through f-k analysis.

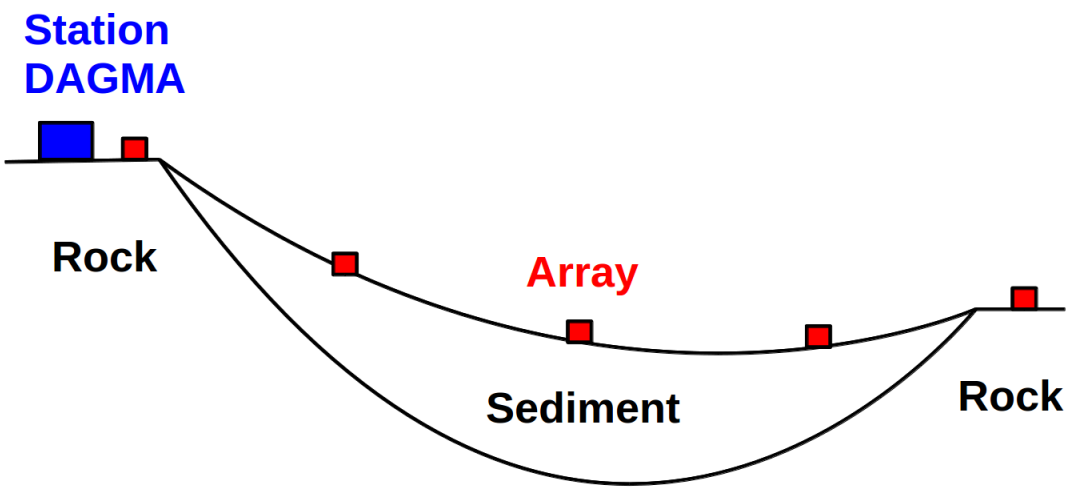

Figure 11 - *Schematic representation of the variability of the quaternary sediment fill over the measuring area. The sediment thickness appears to be maximum near the center of the array, while the bedrock is nearly outcropping at the edges.*

The valley morphology has probably some influence on the directionality of the ambient vibration wave-field at high frequency. This might be related to the geometrical elongation of the quaternary cover along the valley axes. An effect of the topographic slope seems to be unlikely in this case. All stations close to the center of the array are more affected by a certain directionality of the H/Vs at the resonance peak (f_1), which is aligned preferentially along the valley axes (e.g. **Figure 12**C, D). This is nevertheless not surprising, as this phenomenon is widely observed in sedimentary basins. Moving toward the edges of the measurement area, the directionality effect is confined to very high frequencies (e.g. about 30 Hz in **Figure 12**A), and it is therefore negligible for our purposes. At the permanent station, no evidence of directionality is present from the analysis of the H/V spectral ratios (**Figure 12**B).

The result of the directional analysis is also confirmed by applying the wavelet polarization analysis techniques as described in Burjanek et al. (2008) to permanent station DAGMA. Also in this case no sign of directionality (**Figure 13**A) and polarization (**Figure 13**B) of the wave-field are observable.

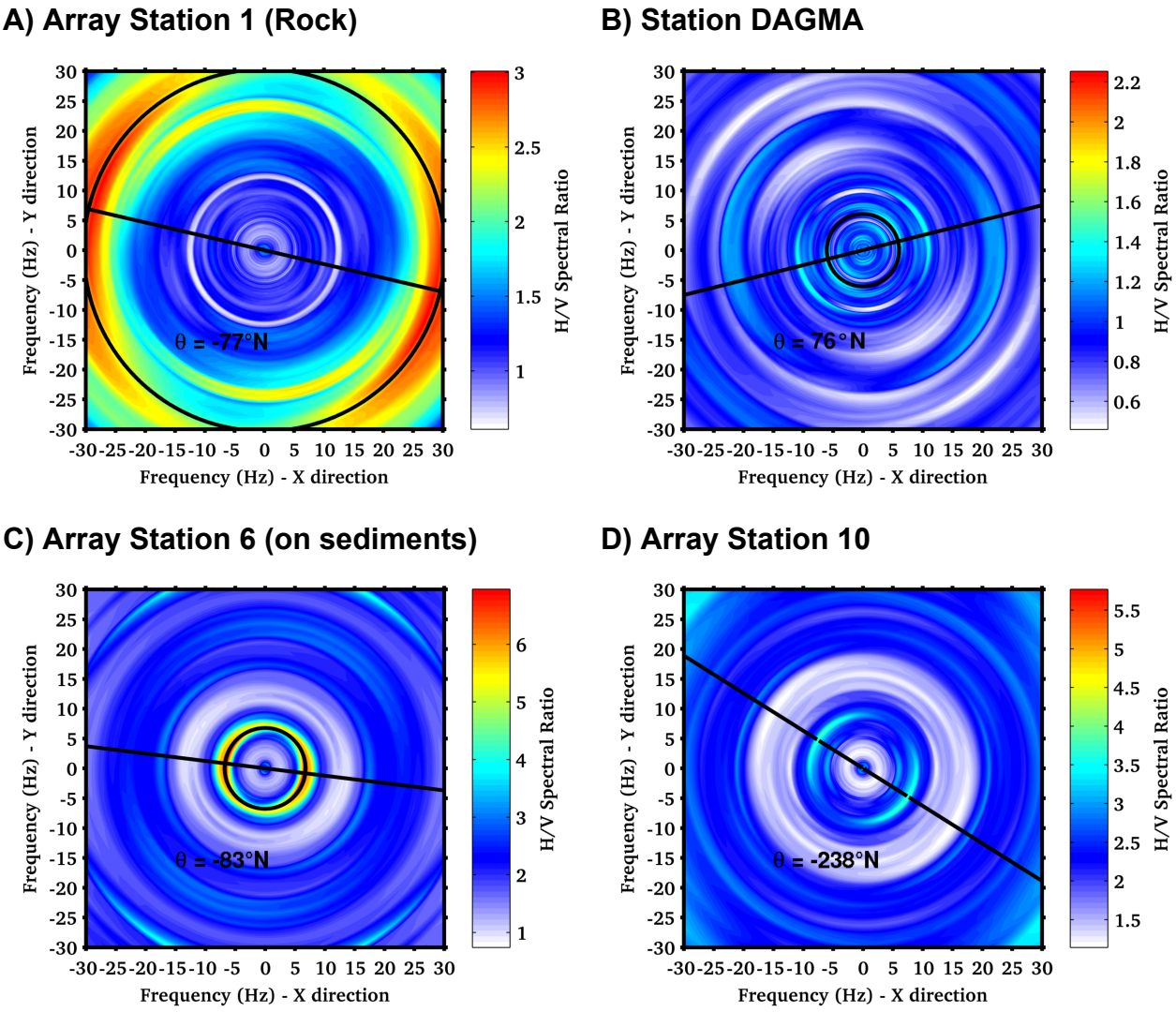

Figure 12 - *Example of directional H/V spectral ratios at three stations of the array and at the permanent station DAGMA. No consistent evidence of wave-field anisotropy is present at low frequency (below 7Hz), while the high frequency resonance peak (f_1, >7Hz) is preferentially aligned along the valley axes, and might be therefore influenced by the geometrical elongation of the quaternary cover.*

A)

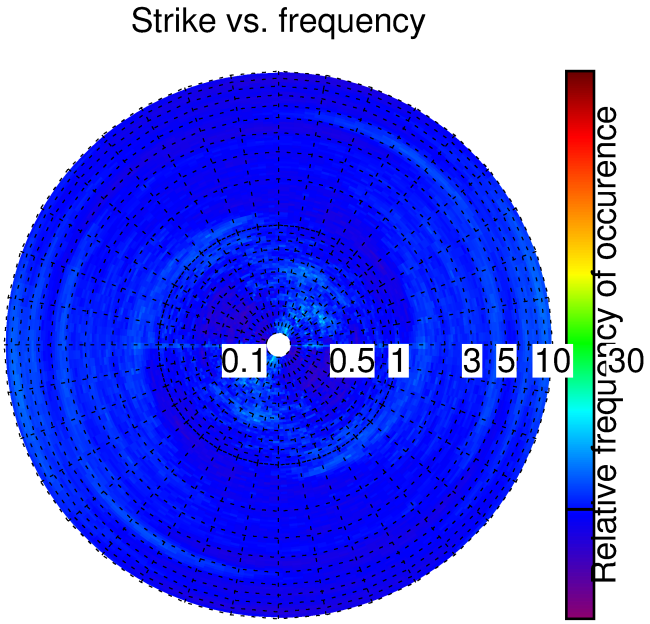

B)

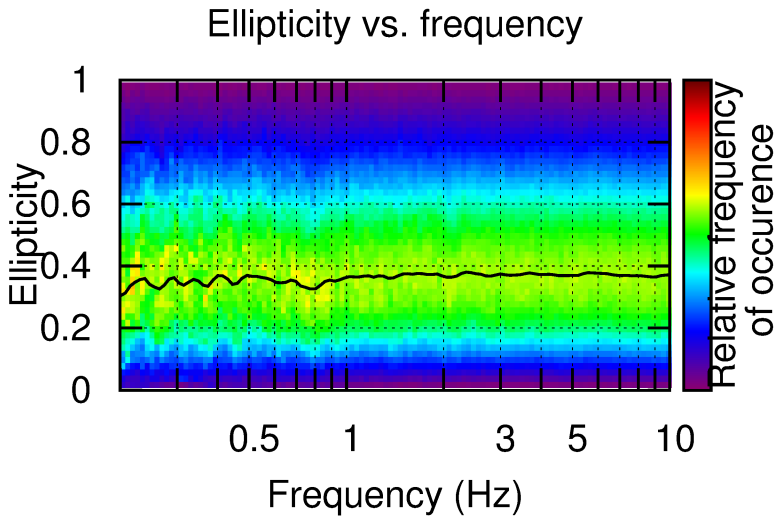

Figure 13 - *Wavelet-based polarization analysis at the permanent station DAGMA. By analyzing the polarization over strike (A) and the particle motion ellipticity plot (B), no directional effect is visible in the frequency range of interest.*

9. Three-component f-k analysis

The frequency-wavenumber analysis is a spectral technique based on seismic array recordings that allows retrieving the direction and the dispersion characteristics of the surface waves. We apply here this technique to three-component ambient vibration recordings using a modification of the high-resolution method of Capon (1969) as described in Poggi et al. (2010). Using all the three-components of motion gives the possibility to retrieve information about the propagation of the Rayleigh waves (vertical and radial processing direction) as well as of the Love waves (transversal direction).

As in the case of the previous methods, the ambient vibration recordings are treated statistically by subdividing the traces in sub-windows. For each consecutive window a separated f-k analysis is performed, and the results are then averaged over the whole recording, increasing the robustness of the final estimation.

As first step, from the f-k analysis it was possible to assess the noise source azimuthal distribution over a range of analyzed frequencies (e.g. **Figure 14**) for the vertical, the radial and the transversal component. A rather uniform (isotropic) distribution is observed for all the components, and particularly in the low frequency range (3-5Hz), confirming then the independency of the noise source distribution to the directional behavior observed in the H/V spectral ratio. Subsequently, the surface-wave dispersion curves are extracted from these distributions by visual inspection and manual picking of the f-k density plots (**Figure 15**).

3-5Hz

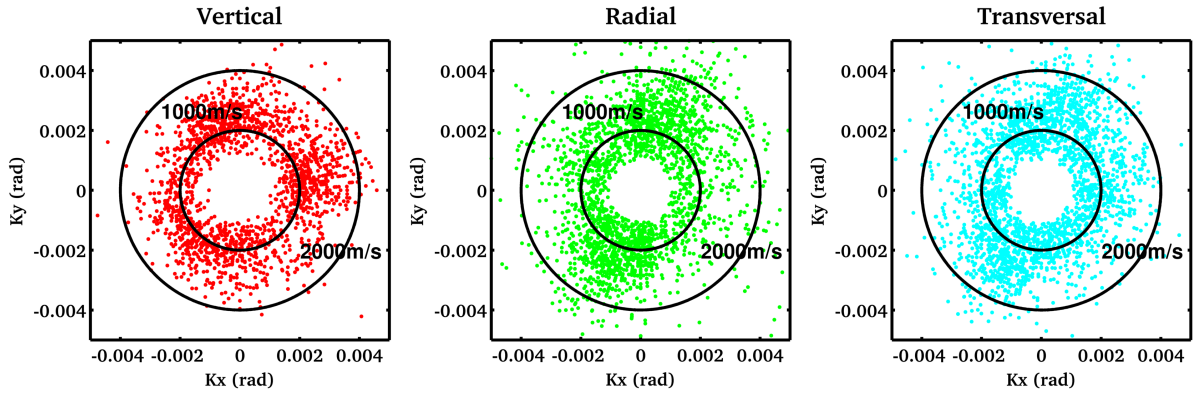

Figure 14 - *Example of distribution of noise sources in the low frequency range (3-5Hz) obtained from three-component f-k analysis. The source distribution is homogenous for all the components in the useful frequency band.*

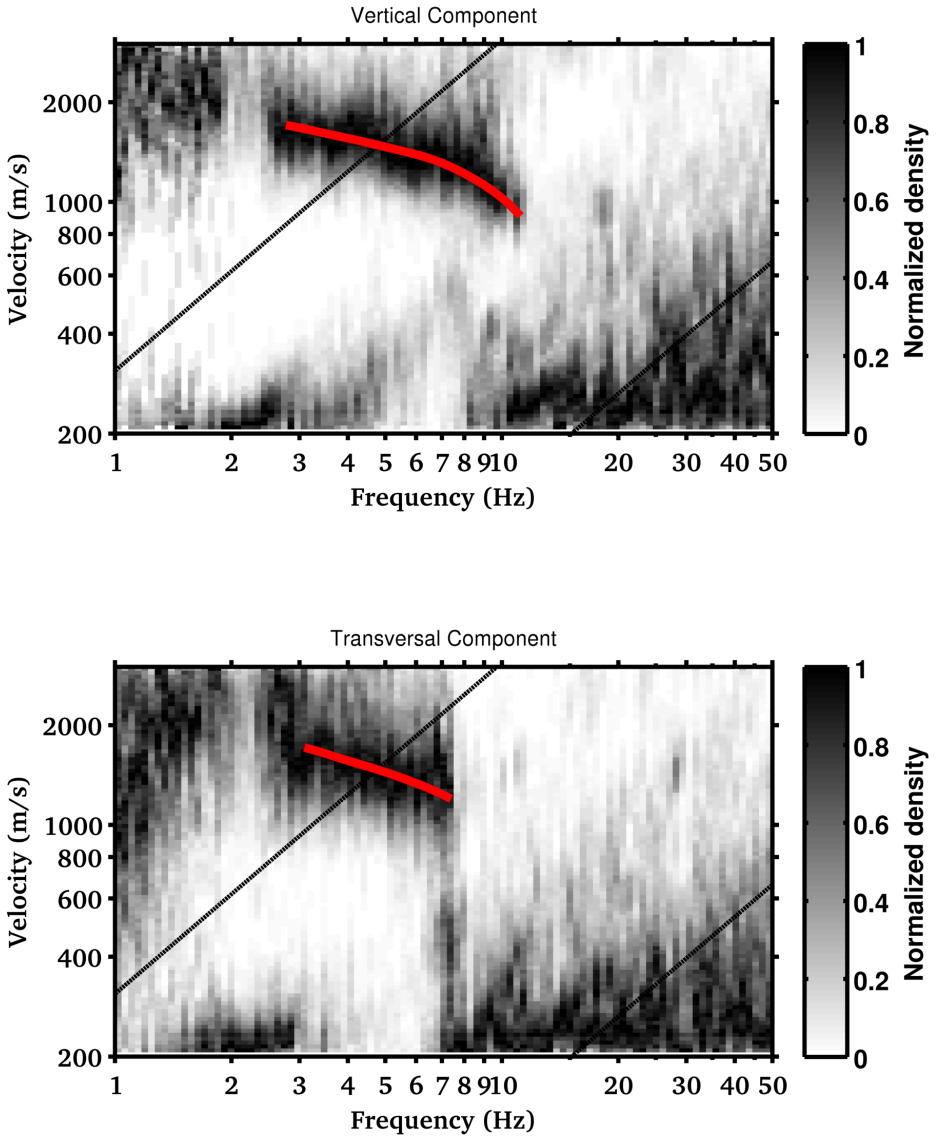

Figure 15 - *Density distribution of the surface wave signals obtained from the recording of the whole DAGMA array using three-component f-k analysis. Top: result from the analysis of the vertical component (Rayleigh waves); Bottom: result for the transverse component (Love waves). In red the interpreted dispersion curves are given (manually selected).*

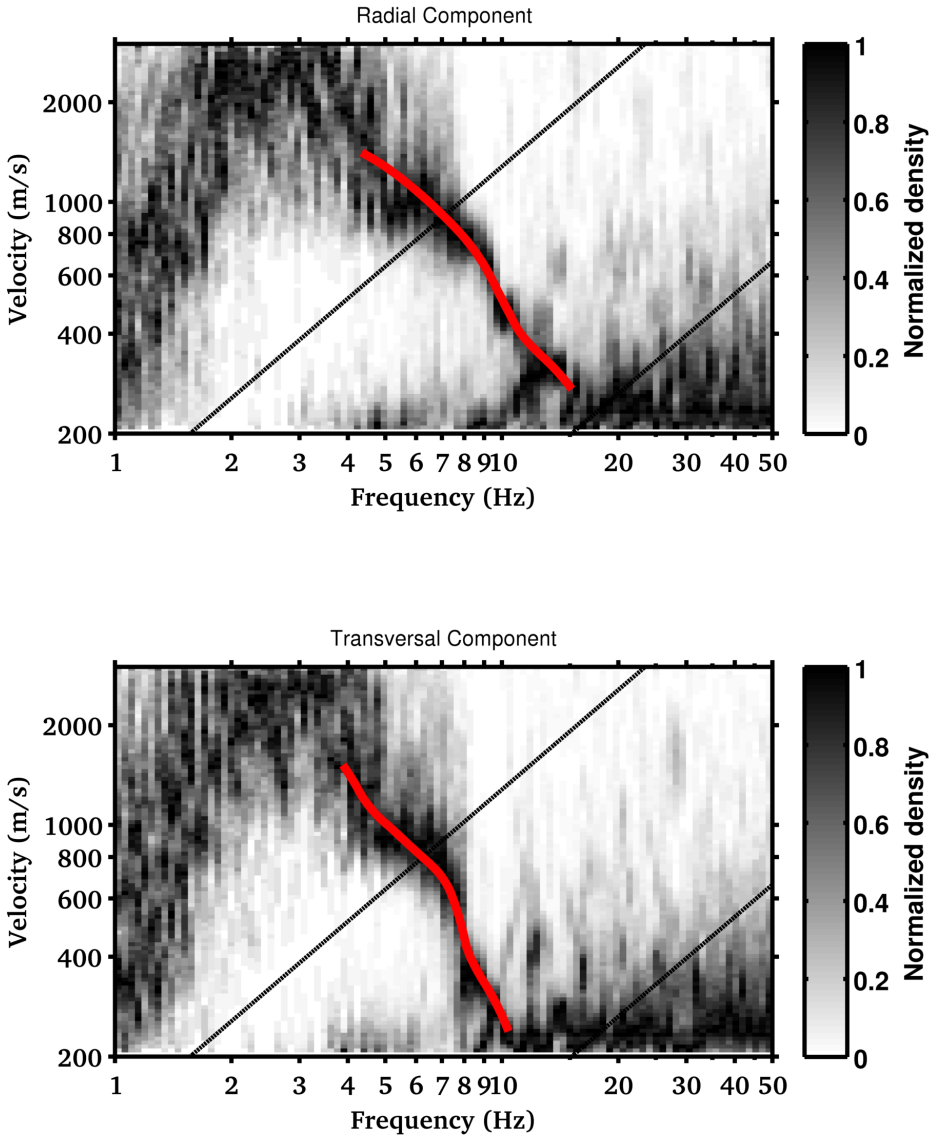

Figure 16 - *Density distribution of the surface wave signals obtained from the recording of the only "inner selection" of the DAGMA array using three-component f-k analysis. Top: result from the analysis of the vertical component (Rayleigh waves); Bottom: result for the transverse component (Love waves). In red the interpreted dispersion curves are given (manually selected).*

In a first attempt, all the receivers of the array have been used, with the only exception of station number 13, which was not properly coupled to the ground. In this case, due to the complex geometrical of the site, the dispersion patterns from soft sediment part and the rock part are interfering, leading to some difficulties in the modal interpretation. In order to isolate the contribution of the quaternary cover from the interpretation, a second test was performed by using the only "inner selection" configuration. This test confirmed the presence of shallow low velocity layers in the central part of the basin and subsequently gave the possibility to correctly isolate and address those portions of dispersion curves related to the bedrock.

We now focus on the rock part only, which is of interest for the characterization of the seismic response at the permanent station. From f-k analysis, the Rayleigh wave dispersion can clearly be tracked between about 3 and 8Hz, as well as the Love waves. The dispersion pattern is typical for a gradient velocity profile, with progressive decrease in velocity with frequency and no evident jump. The final interpretation of the modal dispersion pattern is then presented in **Figure 17** for both the Rayleigh and Love waves, also comparing the rock and the soft sediment model obtained from the inner array sub-selection.

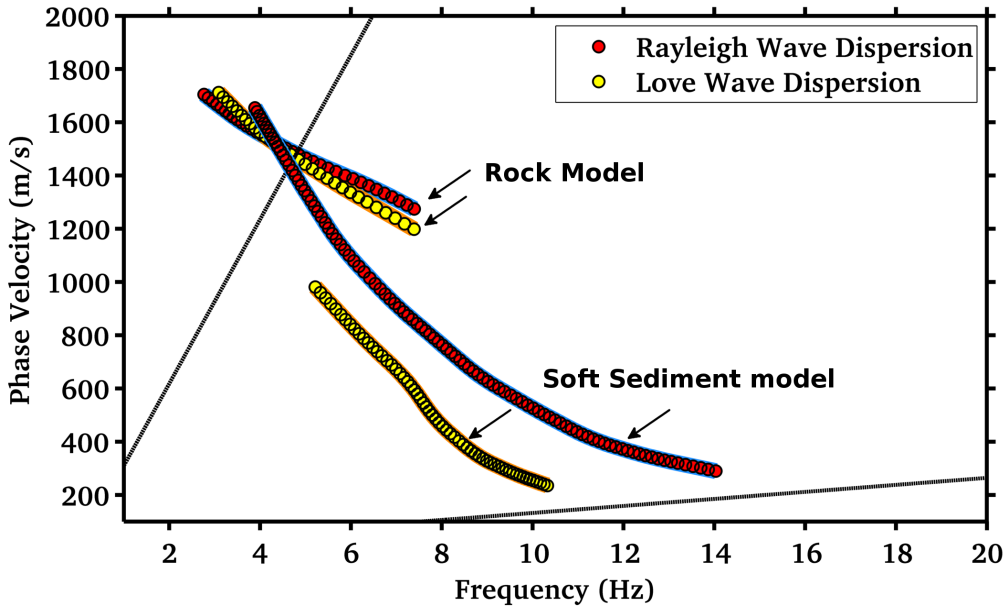

Figure 17 - *Final interpretation of the Rayleigh and Love dispersion curves from the different station selections of the DAGMA array. Minimum and maximum resolution bounds from the full array are indicated with black solid lines.*

10. Inversion of the dispersion curves

The surface wave dispersion curves (Rayleigh and Love) obtained from the three-component f-k analysis of the ambient vibrations were inverted to obtain an estimation of the velocity profile of the site (mainly S-wave velocity as function of depth, and to a lesser extend the P-wave velocity, due to the lower sensitivity). The analysis was performed using the software *Dinver* (www.geopsy.org), which implements a direct search approach (**Figure 18**) based on a conditional version of the neighborhood algorithm (Sambridge, 1999).

To parameterize the velocity model, two different approaches were implemented. The first one consisted in setting up an eight-layer model with free interface depths (**Figure 19**). In such a case the free inversion parameters are then the velocities (P and S) and layer thicknesses. In the second case, a fixed-thickness layer approach was used (**Figure 20**). The advantage of the former method stays in the possibility to better resolve sharp velocity interfaces, while the second is less unique and better constraints the seismic velocity. The two approaches have to be nevertheless considered complementary, and they should provide consistent results. Ten inversion tests (*runs*) have been performed for each of the two model schemes, in order to minimize the effect related to a possible unfavorable initial randomization of the parameter space. Additional ten runs were also performed with the above layering scheme, but using a Montecarlo search instead. This was done as supplementary consistency check, to evaluate the sensitivity of the inverted models, and to identify possible local minima in the parameter space. The best fitting models from of each run were then collected (**Figure 21**) and used later on for the computation of the derived soil parameters.

In more detail, the inverted velocity models (Vs and Vp) are gradient-like, with a faster increase in velocity in the first 20m, followed by a smoother part. This is generally expected for a rock velocity profile. The uppermost velocities of the profile, however, are not directly constrained by the data, because of the lack of information at high frequencies, and might be underestimating the true values for the topmost 10m. This was then confirmed by preliminary computing the SH-wave transfer function from these models, which showed considerable amplitude at high frequencies. It was then decide to introduce an a-priori constraint to the inversion result by homogenizing the top of each model to the velocity found at 10m. This expedient appropriately decreased the amplitude of the amplification function at high frequency, without significantly modifying the fit with observed dispersion curves (**Figure 22**). To have a better constraint on the shallower part of the profile, however, an active seismic experiment might be advisable (e.g. SASW).

Finally, by considering the minimum available frequency of the surface-wave dispersion curves, and by analyzing the scattering of the inverted models (**Figure 21**), it is realistic to assume the velocity profiles to be reliable down to a depth of about 140~160m. Below this value no direct constrain is available, and the velocity are obtained by pure extrapolation.

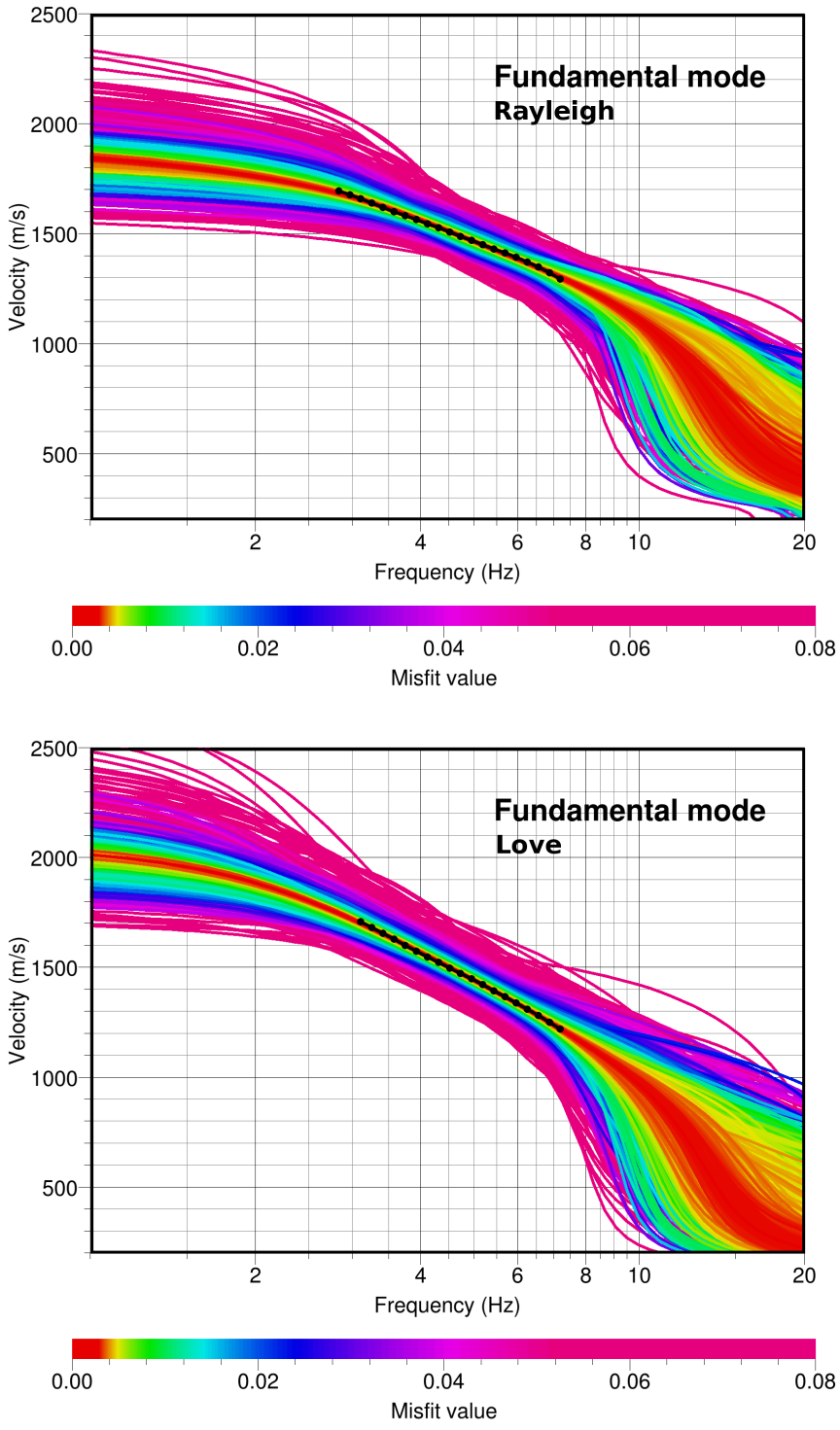

Figure 18 - *Fitting the surface dispersion data within the global optimization procedure. Different colors represent different misfit between the observed (in black) and the modeled dispersion curves during the search.*

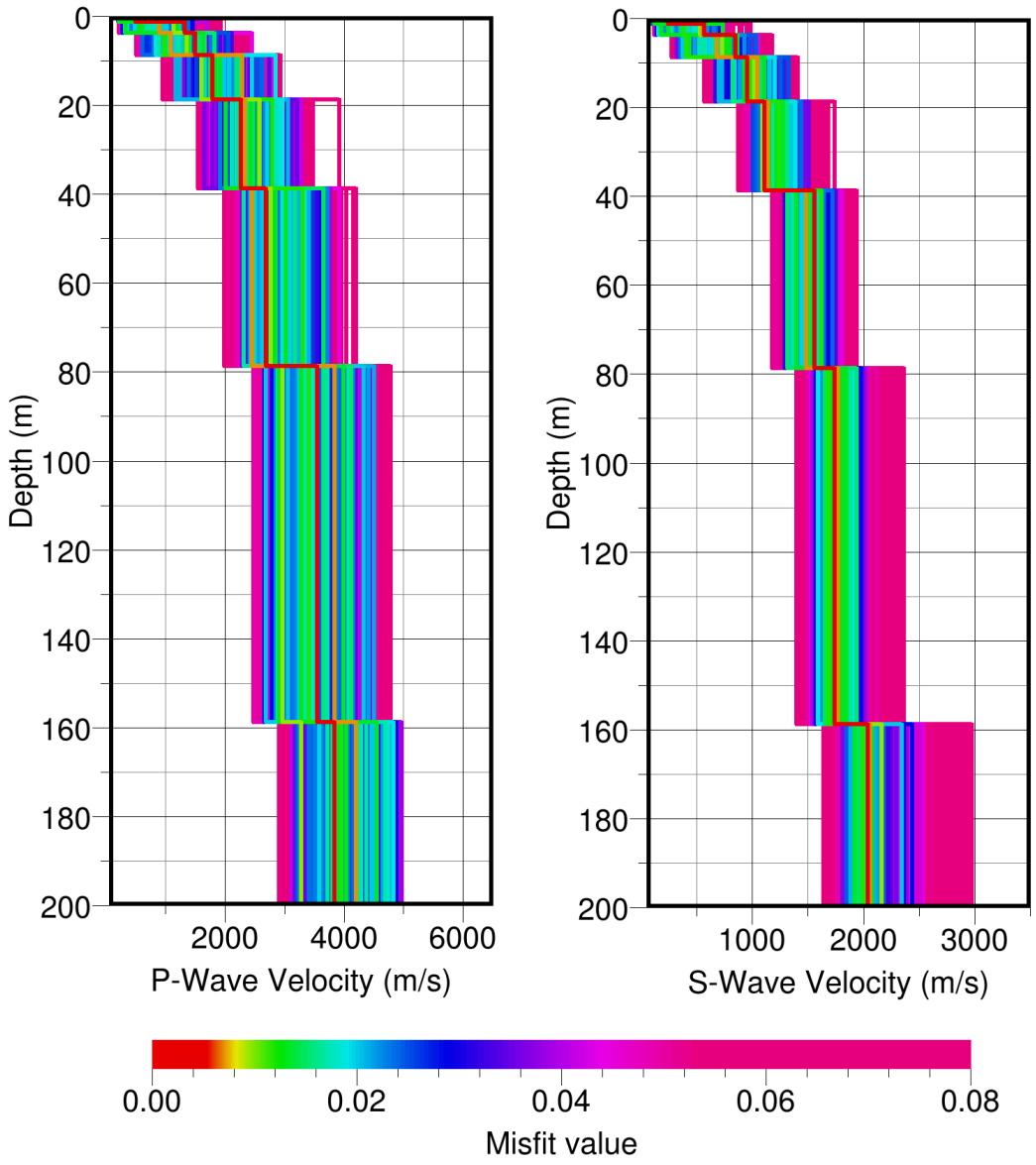

Figure 19 - *Distribution of the fix-layer velocity models generated during the inversion process and ordered by decreasing misfit, according to the color scheme of* **Figure 18**.

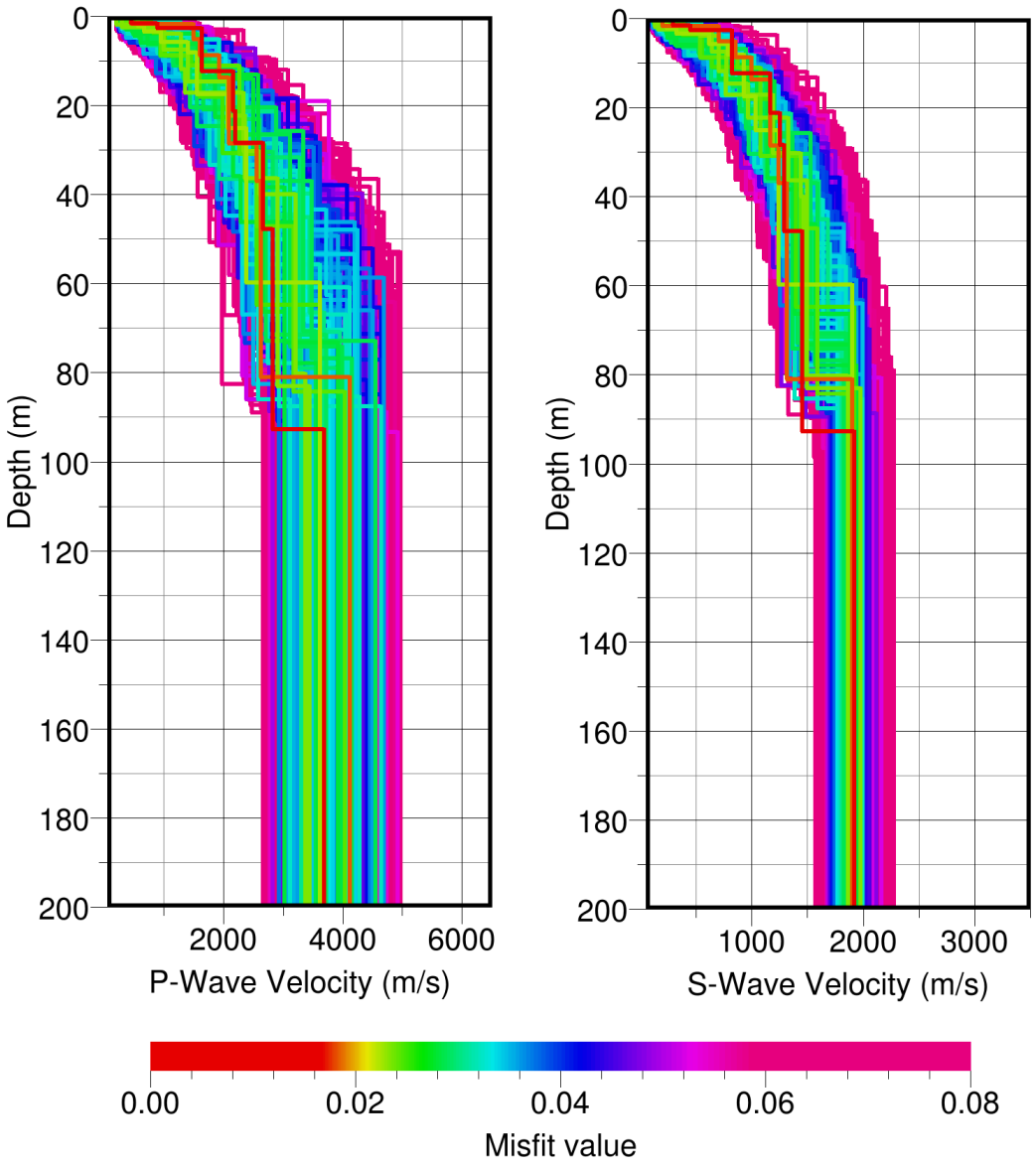

Figure 20 - *Distribution of the free-layer velocity models generated during the inversion process and ordered by decreasing misfit, according to the color scheme of* **Figure 18**.

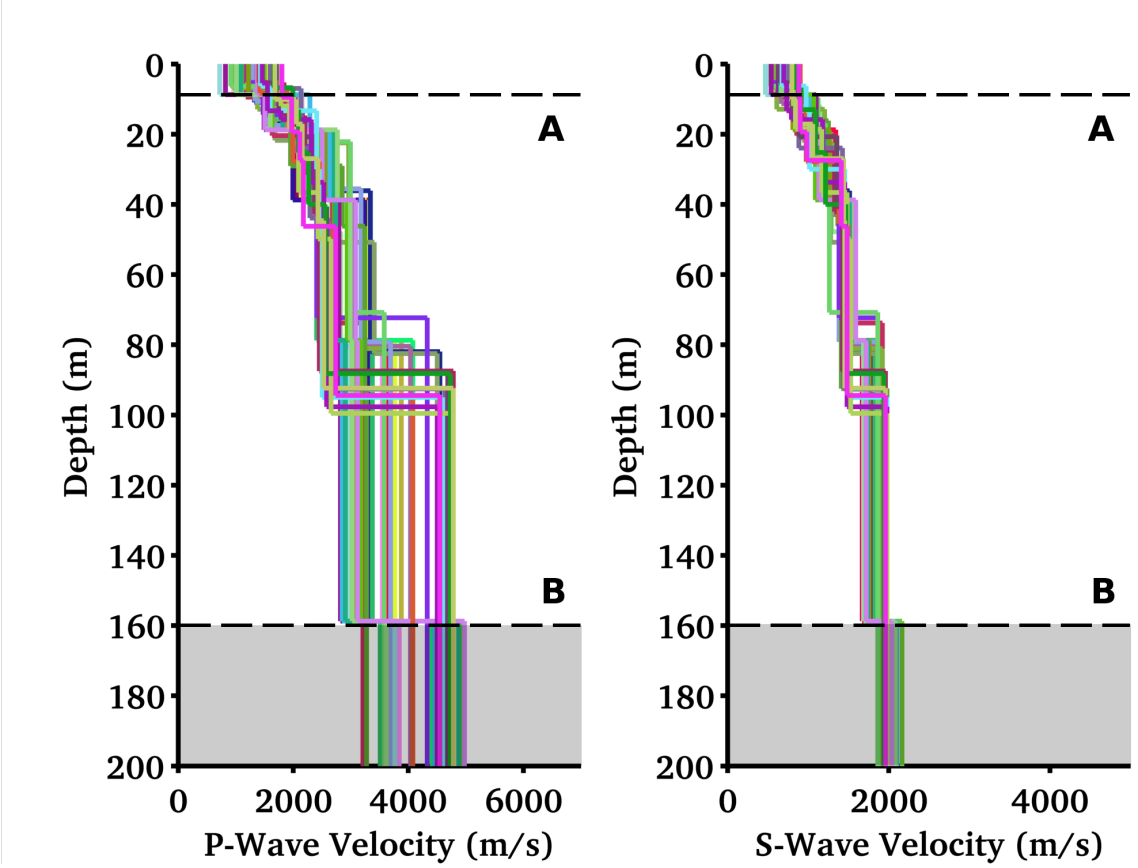

Figure 21 - *Comparison of all the best models from the two parameterization schemes (free and fixed layers). The two approaches are consistent down to a depth of about 140~160m, which can be considered the maximum resolved depth. The topmost layers of each model have also been homogenized at the a-priori depth of 10m.*

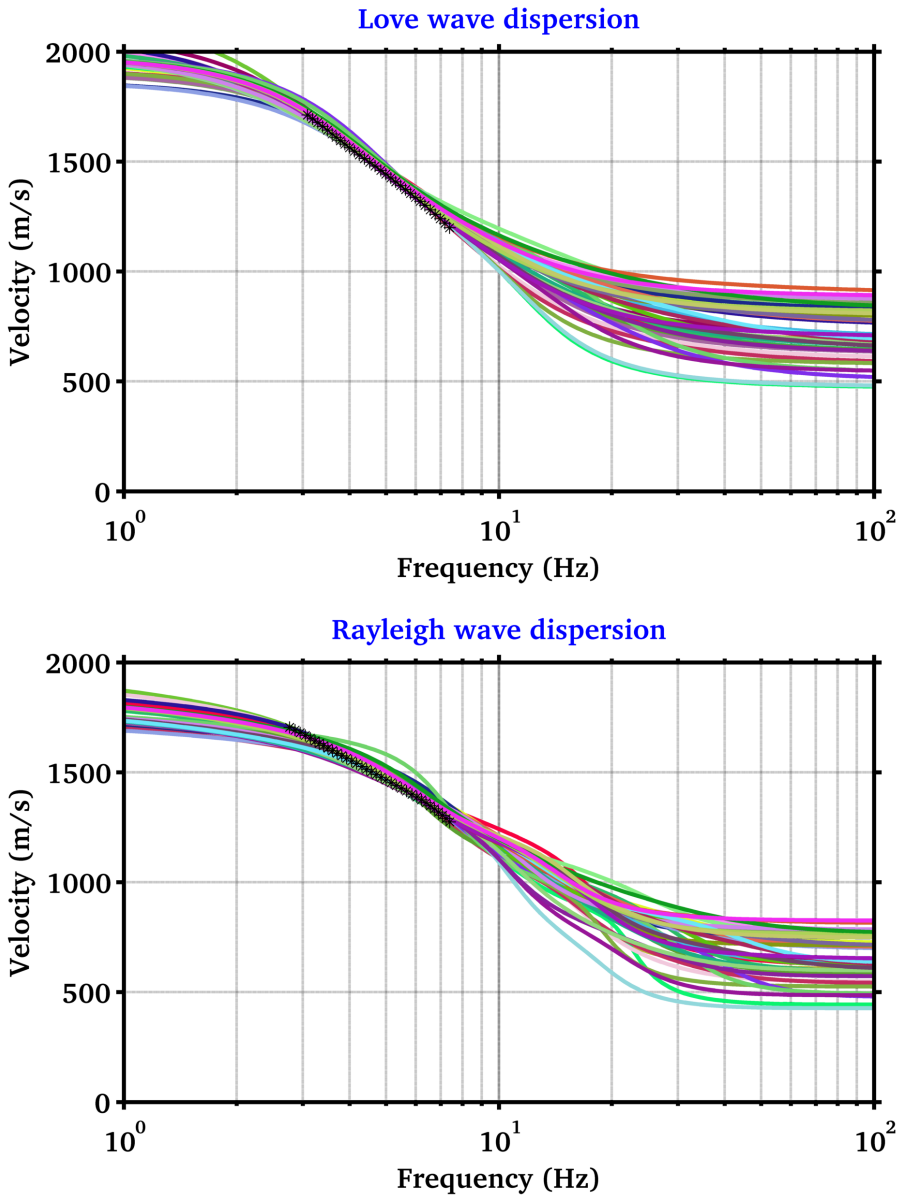

Figure 22 - *Comparison between observed and synthetic dispersion curves, these last computed from the adjusted velocity models of* **Figure 21**. *The introduction of the a-priori selection of minimum and maximum resolved depth does not influence significantly the fitting with empirical data.*

11. Engineering soil parameters

The ensemble of all the best inverted velocity profiles is then used to derive average soil parameters like the VsZ (average travel-time S-wave velocity over the depth Z, including Vs30, Table 1) and the quarter-wavelength (QWL) average velocities (Joyner et al., 1984) for a range of frequencies between 0.6 and 30Hz (**Figure 23**). The former is a standard parameter for the classification of ground-types in most building codes and in ground motion prediction equations. The latter is a parameter useful for the empirical estimation of the site-response and to assess the sensitivity of the seismic wave-field to the different depths. It has to be noticed that these two parameters are derived separately from all the best S-wave velocity models obtained from the inversion, and the results is finally averaged to improve statistics.

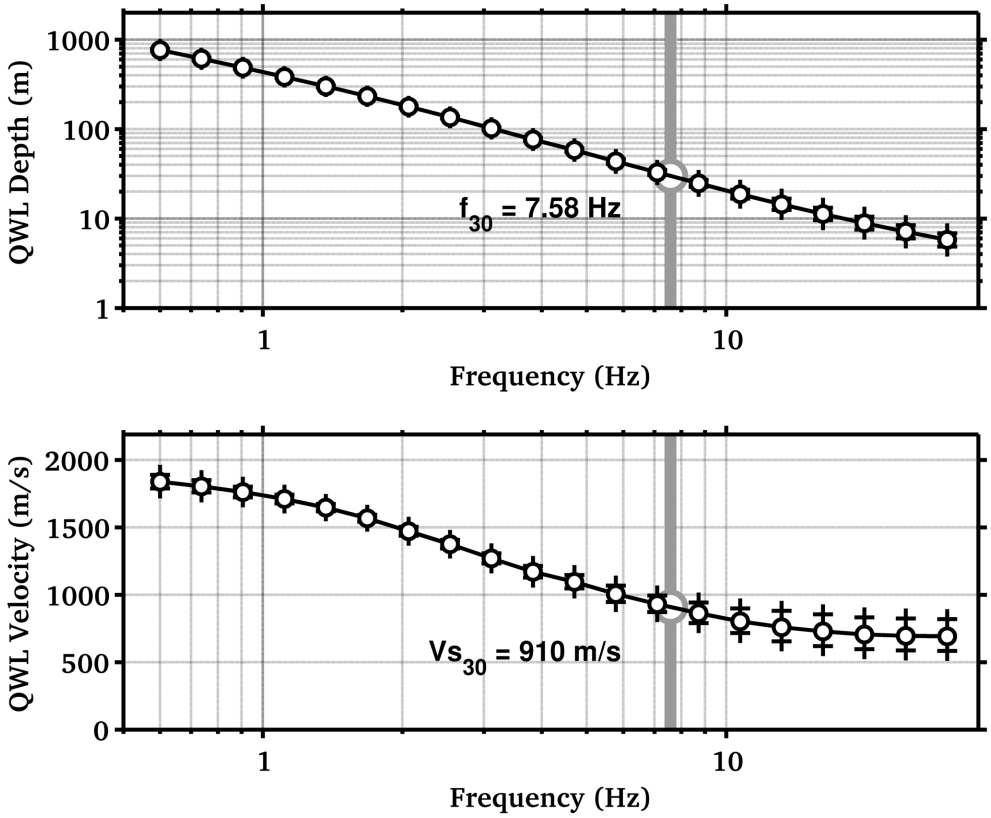

Figure 23 - *Quarter-wavelength representation of the inverted S-wave velocity profiles. Top: the depth-frequency dependency. Bottom: the QWL average velocity. The Vs30 value is indicated with its corresponding QWL frequency.*

Averaging depth	Vs-mean (m/s)	St.Dev.
5	701.25	114.27
10	729.08	98.97
15	779.38	76.98
20	823.92	63.31
25	872.30	52.97
30	**913.70**	**46.88**
40	982.23	42.70
50	1051.84	37.02
75	1167.08	32.34
100	1263.87	25.88
150	1408.94	26.00
200	1515.05	21.53

Table 1 - *Average travel time velocities at different depths. Vs30 is highlighted.*

12. Amplification models

Site amplification functions have been computed using two different approaches: the S-wave transfer function for vertical propagation and the quarter-wavelength amplification. In general the first method is used to evaluate the resonance characteristics of the site, while the second is more useful to assess the effect of the velocity contrasts between the lowermost rock layer (as reference) and the different QWL averaging depths. The two amplification functions are then corrected for the Swiss rock reference velocity profile as defined in Poggi et al. (2011), according to the procedure described in Edwards et al. (2013). Given the lower velocities in the uppermost part of the DAGMA profile compared to the Swiss reference, the final corrected amplification function shows a lower average amplification level at high frequencies than the uncorrected (**Figure 24**).

Amplification functions using the transfer function and the quarter-wavelength approach are comparable (**Figure 25**), even if the transfer function provides a slightly larger amplification, because of the presence of some weak resonance peaks. At low frequencies both methods converge to the same amplification level. It has to be notice that the amplification functions do not include attenuation at this stage of the analysis, as the quality factors of the site are unknown.

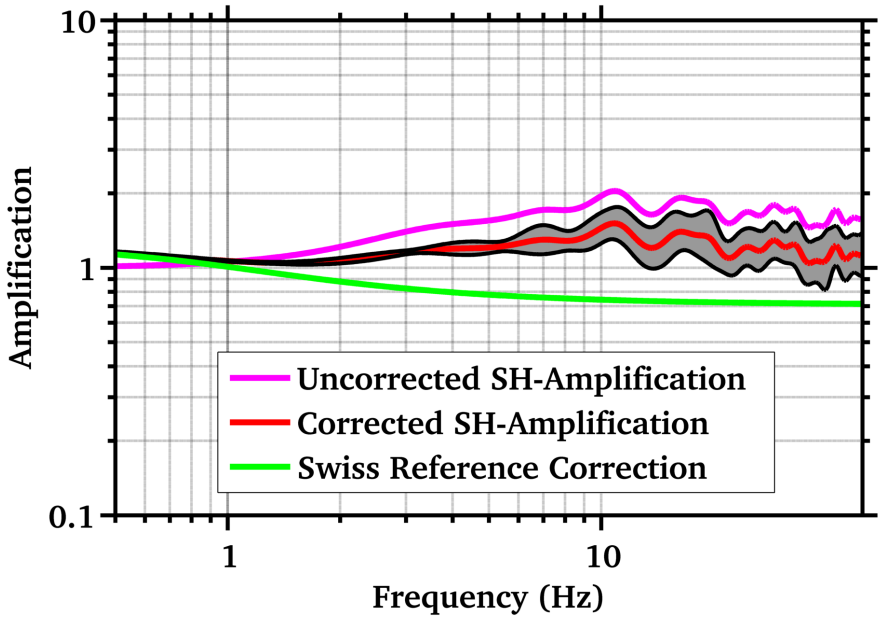

Figure 24 - *Correcting the SH-wave transfer function for the Swiss (rock) reference conditions (Poggi et al. 2011). The final corrected amplification function shows a lower (average) amplification at high frequencies than the uncorrected.*

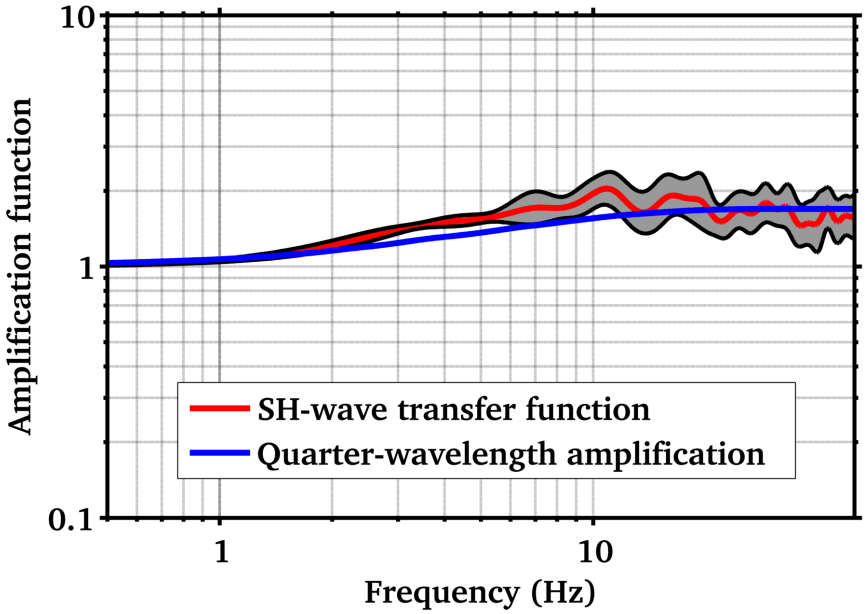

Figure 25 - *Comparison of amplification functions computed using the SH-wave transfer function and the quarter-wavelength formalism on the inverted velocity models. The functions are referenced to the Swiss rock reference model (Poggi et al. 2011).*

REFERENCES

Capon, J., 1969. High resolution frequency wavenumber spectrum analysis, Proc. IEEE, 57, 1408-1418.

Burjanek, J., G. Stamm, V. Poggi, J.R. Moore, and D. Fäh [2010], "Ambient vibration analysis of an unstable mountain slope", Geophys. J. Int., Vol. 180, pp. 820-828.

Edwards, B., C. Michel, V. Poggi and D. Fäh (2013). Determination of Site Amplification from Regional Seismicity: Application to the Swiss National Seismic Networks. Accepted for publication in Seismological Research Letters.

Joyner, W. B., R. E. Warrick and T. E. Fumal (1981). The Effect of Quaternary Alluvium on Strong Ground Motion in the Coyote Lake, California, Earthquake of 1979, Bulletin of the Seismological Society of America, 71, 1333-1349.

Poggi, V., B. Edwards and D. Fäh (2011). Derivation of a Reference Shear-Wave Velocity Model from Empirical Site Amplification, Bulletin of the Seismological Society of America, 101, 258-274.

Poggi, V. and Fäh D., 2010. Estimating Rayleigh wave particle motion from three-component array analysis of ambient vibrations. Geophys. J. Int., 180-1, 251-267.

Huguet. F. (2007). Cirques glaciaires et étagement des formes dans le massif du Feldberg, dans le sud de la Forêt Noire (Allemagne). Géomorphologie: relief, processus, environnement. 4, 309-318.